Research Article

The effect of Nusselt number on the bi-viscosity fluid subjected to the discrete heating effect

M. Adnan ANWAR[1],*⊙**, Mudassar RAZZAQ[1]**⊙

[1]*Department of Mathematics, Lahore University of Management Sciences, Pakistan*

ABSTRACT

Discrete heating action has been established as an energy efficient method. Nusselt number plays a significant role in the heat transfer rate. Local Nusselt number is useful in analyzing the heat transfer rate along the sections of the side walls with different or same temperature in a heated enclosed cavity. Whereas the average Nusselt number quantifies the total heat change in the closed cavity. While the path of the trajectory of the heat flow is being analyzed by heat function. In the current work, multiple heaters of length l_1, l_2 and l_3 are assembled at each side of the isosceles triangle. The numerical simulations of the modeled system along with boundary conditions are carried out by using the standard Galerkin Finite Element Method. The nonlinear algebraic system is solved by Newton method. The behavior of fluid inside the closed triangle with ($Pr = 0.7,10$) is observed. The results are reported in terms of the graphs of the temperature contours, streamlines, average and local Nusselt numbers. The maximum heat transfer rate is observed in convection dominant case. By increasing the magnitude of a bi-viscosity parameter, secondary circulation is observed for $Pr = 10$. The rate of heat transfer has a direct relation with the bi-viscosity parameter. The maximum values of average and local Nusselt numbers are achieved by using the heat generation parameter against the Grashof number.

Cite this article as: M. Adnan A, Mudassar R. The effect of Nusselt number on the bi-viscosity fluid subjected to the discrete heating effect. J Ther Eng 2021;7(7):1797–1814.

INTRODUCTION

In many phenomena of practical approaches, the flow and heat transfer inside a closed cavity have dragged the attention of many authors. As flow and heat transfer expounds the pivotal applications. Convection can be carried out in two different ways: one of them is natural convection and the other is mixed convection. Natural convection is also known as free convection in which the fluid motion inside the cavity is generated only by density differences in the fluid occurring due to temperature gradients. Whereas in mixed convection, convection is carried out by the motion of the boundary wall of the cavity along with gravity and density gradient. Both mechanisms of

*Corresponding author.
E-mail address: adnan.anwar@lums.edu.pk, mudassar.razzaq@lums.edu.pk

convection are constructed by using the fundamental laws of mass, momentum, and energy for the flows of fluids. The behavior of heat transfer inside the cavity depends mainly on the type of convection, fundamental laws, appropriate boundary conditions, and moderate heat transfer rate. The actual solution of governing equations of heat transfer in the cavity is a quite uphill task, so the results are computed via numerical approaches. Eventually, mixed convection can be quantified by unitless parameters: Reynolds, Grashof, and the Prandtl number. Some simulations require the combination of Grashof and Reynolds number. The literature survey of this topic is quite pervasive.

Bondareva in [1] numerically examined the convection melting inside a 2D and 3D enclosure with a heat source. Sivakumar in [2] performed numerical study to analyzed mixed convection heat transfer in a lid driven cavity with discrete heaters of different length and concluded that heat rate enhanced on reducing heating proportion area. Mohamad and Viskanta in [3] reported the three-dimensional flow and heat transfer in a shallow cavity filled with a fluid whose density increase with depth. The top wall was heated and lower was kept cold. Mixed convection heat transfer in an inclined enclosure whose one side was heated, and one side was cool under the impact of the magnetic field. The effect of thermal radiation and heat generation on two-dimensional heat transfer was also analyzed in [4]. Heat transfer in a square cavity with linearly heated side walls was analyzed by Basak, et al. in [5]. Numerical results were computed by using the finite element method. Mixed Convection heat transfer behavior in a square cavity containing porous medium with a movable lid was studied by Basak, et al. in [6], in which all the four walls were kept at different temperatures.

Madhuchhanda Bhattachary, et al. in [7] elaborated on the isothermal and non-isothermal cases of mixed convection heat transfer in the trapezoidal cavity with cold top wall and the hot bottom wall. Ching, et al. see [8] reported the mass and heat transfer with mixed convection in a right triangular enclosure and discussed two cases concerning the direction of motion of the left wall. Basak, et al. in [9] investigated the mixed convection heat flow in a square cavity, whose lower wall heated uniformly and non-uniformly and a top wall was moving at a constant speed. In the case of uniform heating plates, the local Nusselt number showed that the heat transfer at the edges is higher than the rate of heat transfer in the center of the bottom wall. In the non-uniform case, the rate of heat transfer at the edges was observed higher than at the center. A laminar steady state double diffusive mixed convection heat transfer inside a right triangular cavity analyzed by the M. Hasanuzzaman, et al. in [10]. They also expounded on the impact of the Lewis number on the heat and mass transfer. Simulations were carried out by Galerkin weighted residual finite element method. M. Turkyilmazoglu in [11] examined the highly non-linear magnetohydrodynamic viscous fluid flow phenomenon analytically.

In the above-indicated literature survey, Newtonian fluids were taken into consideration. It is natural to think that what will be the effects on thermal efficiency when non-Newtonian fluids are taken inside the cavity. To give the lucid answer of this question, the current study is performed by considering the constitutive equations of the bi-viscosity model. A penalty finite element method on the constitutive equations of the bi-viscosity model is performed to investigate the impact of the discrete heater at the center of walls on the forced convection heat transfer in a triangular cavity. Moreover, the heater at the bottom wall is moving along the positive x-axis direction with uniform velocity. The motivation of the current work is also, due to diverse applications of non-Newtonian fluids. S. Siva Sankaran, et al. in [12] reported the numerical solution of the mixed convection heat transfer in a square cavity with different positions of heaters by using the finite volume method. Magnetohydrodynamics mixed convection heat transfer in a partly heated cavity filled with non-Newtonian fluid was investigated by Fatih, et al. in [13]. A revolving cylinder was subjected at the center of the cavity. The simulations were carried out by using the Galerkin weighted residual finite element method. The mixed convection heat flow behavior in a square cavity subjected to the heater at the bottom wall with a top cold wall, and movable sidewall, filled with nanofluid was expounded by the Sebdani, et al. in [14]. The effect of shear force was examined by keeping the buoyancy force constant and vice versa. The numerical approximation was made to elaborate the combined convection impact on the heat transfer in an open square cavity. The left wall of the cavity is heated, fully or partly with a uniform heating source. The observation was also made between the relationship of the length of the heater and Hartman number [15]. Ali, et al. in [16] examined the mixed convection heat transfer in a triangular cavity with a moving heated lower wall at constant speed filled with a non-Newtonian fluid. The simulation was carried out by using a Galerkin finite element method. Debayan Das, et al. in [17] analyzed the relationship between the number of heaters and thermal efficiency. Double heaters were subjected to each sidewall of the cavities (square and triangular) yields the higher thermal efficiency in contrast to the single heater. Simulations were carried out by a Galerkin finite element method in [18]. In a further study, they examined the impact of the position of multiple heaters on the local Nusselt number. Heat transfer in porous triangular and square enclosures with discrete double heaters along the vertical or inclined walls were elaborated in [19].

MATHEMATICAL MODEL

In the present study, a mixed convection problem is considered in a triangular geometry. Figure 1 illustrates the coordinate systems and geometry of given problems. The flow is assumed to be steady two dimensional in a triangular
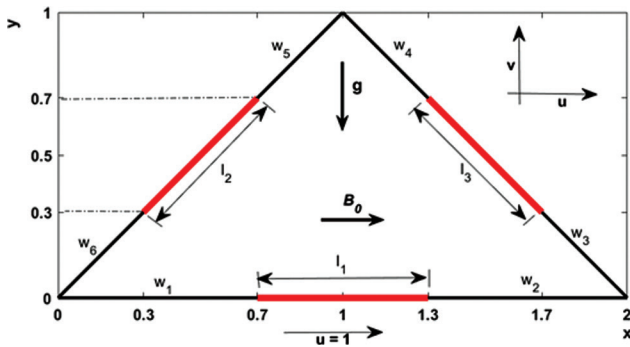
Figure 1. Geometry of the flow problem.

shaped cavity filled with viscous fluid. Three heaters l_1, l_2 and l_3 are placed at the center of each wall as shown in Figure 1. These heaters have uniform temperature θ_h. While temperature at w_1, w_2, w_3, w_4, w_5 and w_6 is θ_c (cold walls). The bottom heater l_1 moves in positive x direction. A uniform magnetic field is also applied in positive x direction.

So, there are three factors that caused the fluid motion inside triangle. Which are moving heater, density difference and gravity force. Due to different temperature along the walls, density difference arises. These factors (gravity and density) produce buoyancy force. The constitutive relation related to the bi-viscosity fluid, see in [20], can be written as:

$$\vec{\theta} = -p\mathbf{I} + \vec{\tau}, \tag{1}$$

where,

$$\vec{\tau} = \begin{cases} 2\left(\mu_b + \dfrac{P_y}{\sqrt{2\Pi}}\right)\overrightarrow{\mathbf{A_1}}; & \pi < \pi_c, \\[3mm] 2\left(\mu_b + \dfrac{P_y}{\sqrt{2\Pi_c}}\right)\overrightarrow{\mathbf{A_1}}; & \pi > \pi_c. \end{cases}$$

It is remarkable that the matter will act as solid for $\pi < \pi_c$ and it performs as fluid for $\pi > \pi_c$. Considering above deliberation, the governing system of this problem becomes:

$$\frac{\partial \vec{u}}{\partial \vec{x}} + \frac{\partial \vec{v}}{\partial \vec{y}} = 0, \tag{2}$$

$$\vec{u}\frac{\partial \vec{u}}{\partial \vec{x}} + \vec{v}\frac{\partial \vec{u}}{\partial \vec{y}} = -\frac{1}{\rho}\frac{\partial \vec{p}}{\partial \vec{x}} + \frac{\overline{\mu_b}}{\rho}\left(1 + \frac{1}{\beta}\right)$$
$$\left(\frac{\partial^2 \vec{u}}{\partial \vec{x}^2} + \frac{\partial^2 \vec{v}}{\partial \vec{y}^2}\right), \tag{3}$$

$$\vec{u}\frac{\partial \vec{v}}{\partial \vec{x}} + \vec{v}\frac{\partial \vec{v}}{\partial \vec{y}} = -\frac{1}{\rho}\frac{\partial \vec{p}}{\partial \vec{x}} + \frac{\overline{\mu_b}}{\vec{\rho}}\left(1 + \frac{1}{\beta}\right)$$
$$\left(\frac{\partial^2 \vec{v}}{\partial \vec{x}^2} + \frac{\partial^2 \vec{v}}{\partial \vec{y}^2}\right) + \vec{g}\,\overline{\beta_0}(\vec{\theta} - \overline{\theta_c}) - \frac{\sigma B_0 \vec{v}}{\vec{\rho}}, \tag{4}$$

$$\vec{u}\frac{\partial \vec{\theta}}{\partial \vec{x}} + \vec{v}\frac{\partial \vec{\theta}}{\partial \vec{y}} = \alpha\left(\frac{\partial^2 \vec{\theta}}{\partial \vec{x}^2} + \frac{\partial^2 \vec{\theta}}{\partial \vec{y}^2}\right)$$
$$+ \frac{Q}{\rho c_p}(\vec{\theta} - \overline{\theta_c}) - \frac{4}{3}\frac{1}{\rho c_p}\left(\frac{\partial \overrightarrow{q_{rx}}}{\partial \vec{x}} + \frac{\partial \overrightarrow{q_{ry}}}{\partial \vec{y}}\right). \tag{5}$$

The boundary conditions of the considered flow problem are defined by

$$\vec{u} = U_0, \quad \vec{v} = 0, \quad \vec{\theta} = \overline{\theta_h}, \quad \text{on} \quad 0 \le \vec{x} \le 2l,$$
$$\text{and} \quad \vec{y} = 0,$$

$$\vec{u} = 0, \quad \vec{v} = 0, \quad \vec{\theta} = \overline{\theta_h} - (\overline{\theta_h} - \overline{\theta_c})\frac{\vec{y}}{l}, \quad \text{on} \quad \vec{x} = \vec{y},$$
$$\text{and} \quad 0 \le \vec{x} \le l, \quad 0 \le \vec{y} \le l, \tag{6}$$

$$\vec{u} = 0, \quad \vec{v} = 0, \quad \vec{\theta} = \overline{\theta_h} - (\overline{\theta_h} - \overline{\theta_c})\frac{\vec{y}}{l}, \quad \text{on} \quad \vec{y} = 2l - \vec{x},$$
$$l \le \vec{x} \le 2l, \quad 0 \le \vec{y} \le l.$$

The Eq. (2) is the continuity equation, also called incompressible condition, Eqs. (3) and (4) are momentum equations, Eq. (5) is the heat equation. The radiative heat flux is defined as:

$$q_{rx} = -(4\sigma/3k^*)(\partial \theta^4/\partial x),$$
$$q_{ry} = -(4\sigma/3k^*)(\partial \theta^4/\partial y). \tag{7}$$

Assume that, the temperature difference within the flow fluid is small. So expending θ^4 by using Taylor series about θ_c gives $\theta^4 = 4\theta_c^3\theta - 3\theta_c^4$. Establish the dimensionless parameters:

$$x = \frac{\vec{x}}{l}, \quad y = \frac{\vec{y}}{l}, \quad u = \frac{\vec{u}}{U_0}, \quad v = \frac{\vec{v}}{U_0}, \quad T = \frac{\vec{\theta} - \overline{\theta_c}}{\overline{\theta_k} - \overline{\theta_c}},$$

$$p = \frac{\vec{p}}{\rho U_0^2}, \quad Pr = \frac{\vec{v}}{\alpha}, \quad \epsilon = \frac{Ql^2}{k},$$

$$Re = \frac{U_0 l}{\vec{v}}, \quad N_R = \frac{4\sigma\theta_c^3}{kk^*}, \quad Gr = \frac{\vec{g}\,\overline{\beta_0}(\overline{\theta_h} - \overline{\theta_c})l^3}{\vec{v}^2},$$

$$Ha^2 = \frac{\sigma B_0^2 l^2}{\mu}, \quad Ri = \frac{Gr}{Re^2}. \tag{8}$$

The Eqs. (2) – (5) and boundary conditions defined in Eq. 6, takes the following form:

$$\frac{\partial u}{\partial x} + \frac{\partial v}{\partial y} = 0, \tag{9}$$

$$u\frac{\partial u}{\partial x} + v\frac{\partial u}{\partial y} = -\frac{\partial p}{\partial x} + \frac{1}{Re}\left(1 + \frac{1}{\beta}\right)$$
$$\left(\frac{\partial^2 u}{\partial x^2} + \frac{\partial^2 v}{\partial y^2}\right), \tag{10}$$

$$u\frac{\partial v}{\partial x}+v\frac{\partial v}{\partial y}=-\frac{\partial p}{\partial x}+\frac{1}{Re}\Big(1+\frac{1}{\beta}\Big)$$
$$\Big(\frac{\partial^2 v}{\partial x^2}+\frac{\partial^2 v}{\partial y^2}\Big)+RiT-\frac{Ha^2}{Re}v, \tag{11}$$

$$u\frac{\partial T}{\partial x}+v\frac{\partial T}{\partial y}=\frac{1}{Pe}\Big[\Big(1+\frac{4}{3}N_R\Big)$$
$$\Big(\frac{\partial^2 T}{\partial x^2}+\frac{\partial^2 T}{\partial y^2}\Big)+\epsilon T\Big]. \tag{12}$$

The velocity and temperature boundary conditions within the cavity can be expressed as follow:

$$U=1, \quad V=0, \quad T=1, \quad on \quad 1.3\le x\le 1.7$$
$$and \quad y=0,$$
$$U=0, \quad V=0, \quad T=1, \quad on \quad 0.3\le x\le 0.7$$
$$and \quad y=x,$$
$$U=0, \quad V=0, \quad T=1, \quad on \quad 1.3\le x\le 1.7 \tag{13}$$
$$and \quad y=2-x,$$
$$U=0, \quad V=0, \quad T=0, \quad on \quad w_1,w_2,w_3,w_4,w_5$$
$$and \quad w_6.$$

The velocity components u and v are subjected to the no-slip boundary conditions. To analyze the energy efficiency researchers suggested the study of thermal boundary conditions on the cavity.

SOLUTION PROCEDURE

The governing equations (9)–(12) are approximated numerically by using Galerkin Finite Element Method with boundary conditions stated in (13). In order to penalize the pressure term in flow model the Penalty finite element method [21], [22] is applied by using Penalty parameter γ given below:

$$p=-\gamma\Big(\frac{\partial v}{\partial x}+\frac{\partial v}{\partial y}\Big). \tag{14}$$

Eqs. (10) and (11) can be written as follows by using (14)

$$u\frac{\partial u}{\partial x}+v\frac{\partial u}{\partial y}=\gamma\Big(\frac{\partial^2 u}{\partial x^2}+\frac{\partial^2 v}{\partial x\partial y}\Big)$$
$$+\frac{1}{Re}\Big(1+\frac{1}{\beta}\Big)\Big(\frac{\partial^2 u}{\partial x^2}+\frac{\partial^2 u}{\partial y^2}\Big), \tag{15}$$

$$u\frac{\partial v}{\partial x}+v\frac{\partial v}{\partial y}=\gamma\Big(\frac{\partial^2 u}{\partial y\partial x}+\frac{\partial^2 v}{\partial y^2}\Big)$$
$$+\frac{1}{Re}\Big(1+\frac{1}{\beta}\Big)\Big(\frac{\partial^2 v}{\partial x^2}+\frac{\partial^2 v}{\partial y^2}\Big)+RiT-\frac{Ha^2}{Re}v. \tag{16}$$

The weak formulations of the Eqs. (12) and (15) – (16), on the element of Ω with the weight functions η_1, η_2 and η_3 are:

$$\int_{\Omega^\epsilon}\eta_1\Big(u\frac{\partial u}{\partial x}+v\frac{\partial u}{\partial y}\Big)d\Omega-\int_{\Omega^\epsilon}\eta_1\gamma\Big(\frac{\partial^2 u}{\partial x^2}+\frac{\partial^2 v}{\partial y\partial x}\Big)$$
$$-\frac{1}{Re}\Big(1+\frac{1}{\beta}\Big)\int_{\Omega^\epsilon}\eta_1\Big(\frac{\partial^2 u}{\partial x^2}+\frac{\partial^2 u}{\partial y^2}\Big)d\Omega=0,$$

$$\int_{\Omega^\epsilon}\eta_2\Big(u\frac{\partial v}{\partial x}+v\frac{\partial v}{\partial y}\Big)d\Omega-\int_{\Omega^\epsilon}\eta_2\gamma\Big(\frac{\partial^2 u}{\partial x\partial y}+\frac{\partial^2 v}{\partial y\partial x}\Big)$$
$$-\frac{1}{Re}\Big(1+\frac{1}{\beta}\Big)\int_{\Omega^\epsilon}\eta_2\Big(\frac{\partial^2 v}{\partial x^2}+\frac{\partial^2 v}{\partial y^2}\Big)d\Omega \tag{17}$$
$$-Ri\int_{\Omega^\epsilon}\eta_2 Td\Omega+\frac{Ha^2}{Re}\int_{\Omega^\epsilon}\eta_2 vd\Omega=0,$$

$$\int_{\Omega^\epsilon}\eta_3 u\Big(\frac{\partial T}{\partial x}+v\frac{\partial T}{\partial y}\Big)d\Omega-\frac{1}{Pe}\Big(\int_{\Omega^\epsilon}\eta_3\Big(1+\frac{4}{3}N_R\Big)$$
$$\Big(\frac{\partial^2 T}{\partial x^2}+\frac{\partial^2 T}{\partial y^2}\Big)d\Omega-\epsilon\int_{\Omega^\epsilon}\eta_3 Td\Omega\Big)=0.$$

Where the subscript Ω^ϵ on the integral demonstrates that the integral is being calculated over the given triangular cavity i.e. the notion Ω^ϵ the limit of integration. Where η_1, η_2 and η_3 are trial functions.

Here, $u(x,y)$, $v(x,y)$ and $T(x,y)$ are approximated by the finite element interpolations u^e, v^e and T^e over the triangular elements ψ^e,

$$u\approx\sum_{i=1}^{6}u_i^e\psi_i^e(x,y), \quad v\approx\sum_{i=1}^{6}v_i^e\psi_i^e(x,y),$$
$$T\approx\sum_{i=1}^{6}T_i^e\psi_i^e(x,y), \tag{18}$$

where, ψ_i^e trial function defined on the six nodal triangular elements. By Substitution of Eq. (18) into the weak formulation, the j_{th} equation of the finite element model becomes:

$$R_j^{(1)}=\sum_{i=1}^{6}u_i^e\int_{\Omega^\epsilon}\Big\{\Big(\sum_{i=1}^{6}u_i^e\psi_i^e\Big)\frac{\partial\psi_i^e}{\partial x}+\Big(\sum_{i=1}^{6}v_i^e\psi_i^e\Big)\frac{\partial\psi_i^e}{\partial y}\Big\}\psi_j^e d\Omega$$
$$+\gamma\Big\{\sum_{i=1}^{6}u_i^e\int_{\Omega^\epsilon}\frac{\partial\psi_j^e}{\partial x}\frac{\partial\psi_i^e}{\partial x}d\Omega+\sum_{i=1}^{6}v_i^e\int_{\Omega^\epsilon}\frac{\partial\psi_j^e}{\partial x}\frac{\partial\psi_i^e}{\partial y}d\Omega\Big\}$$
$$+\frac{1}{Re}\Big(1+\frac{1}{\beta}\Big)\sum_{i=1}^{6}u_i^e\int_{\Omega^\epsilon}\Big\{\frac{\partial\psi_j^e}{\partial x}\frac{\partial\psi_i^e}{\partial x}+\frac{\partial\psi_j^e}{\partial y}\frac{\partial\psi_i^e}{\partial y}\Big\},$$

$$R_j^{(2)}=\sum_{i=1}^{6}v_i^e\int_{\Omega^\epsilon}\Big\{\Big(\sum_{i=1}^{6}u_i^e\psi_i^e\Big)\frac{\partial\psi_i^e}{\partial x}+\Big(\sum_{i=1}^{6}v_i^e\psi_i^e\Big)\frac{\partial\psi_i^e}{\partial y}\Big\}\psi_j^e d\Omega$$
$$+\gamma\Big\{\sum_{i=1}^{6}\frac{\partial\psi_j^e}{\partial y}\frac{\partial\psi_i^e}{\partial x}d\Omega+\sum_{i=1}^{6}v_i^e\int_{\Omega^\epsilon}\frac{\partial\psi_j^e}{\partial x}\frac{\partial\psi_i^e}{\partial y}d\Omega\Big\}$$

$$+\frac{1}{Re}\left(1+\frac{1}{\beta}\right)\sum_{i=1}^{6}v_i^e\int_{\Omega^e}\left\{\frac{\partial\psi_j^e}{\partial x}\frac{\partial\psi_i^e}{\partial x}+\frac{\partial\psi_j^e}{\partial y}\frac{\partial\psi_i^e}{\partial y}\right\}$$

$$-Ri\int_{\Omega^e}\sum_{i=1}^{6}T_i^e\psi_i^e\,d\Omega+\frac{Ha^2}{Re}\int_{\Omega^e}\sum_{i=1}^{6}v_i^e\psi_i^e\,d\Omega,$$

$$R_j^{(3)}=\sum_{i=1}^{6}T_i^e\int_{\Omega^e}\left\{\left(\sum_{i=1}^{6}u_i^e\psi_i^e\right)\frac{\partial\psi_i^e}{\partial x}+\left(\sum_{i=1}^{6}v_i^e\psi_i^e\right)\frac{\partial\psi_i^e}{\partial y}\right\}\psi_j^e\,d\Omega$$

$$+\frac{1}{Pe}\left(1+\frac{4}{3}N_R\right)\sum_{i=1}^{6}T_i^e\int_{\Omega^e}\left\{\frac{\partial\psi_j^e}{\partial x}\frac{\partial\psi_i^e}{\partial x}+\frac{\partial\psi_j^e}{\partial y}\frac{\partial\psi_i^e}{\partial y}\right\}$$

$$-\frac{1}{Pe}\epsilon\int_{\Omega^e}T_i^e\psi_i^e\,d\Omega.$$

POST PROCESSING: STREAMFUNCTION AND NUSSELT NUMBER

Stream function Ψ exhibit the motion of fluid in the geometry. The relation between stream function Ψ and velocity components (U_X,U_Y) are given as below:

$$U_X=\frac{\partial\Psi}{\partial Y}\quad and\quad U_Y=\frac{\partial\Psi}{\partial X},\qquad(19)$$

from above equation, we can write as follows:

$$\frac{\partial^2\Psi}{\partial Y^2}+\frac{\partial^2\Psi}{\partial X^2}=\frac{\partial U_X}{\partial Y}-\frac{\partial U_Y}{\partial X}.\qquad(20)$$

The positive value of Ψ refers to the anticlockwise circulation, likewise the negative value of Ψ means clockwise circulation. Since we are using a no-slip boundary condition, so the value of stream function near the wall is zero.

Nusselt Number is a leading dimensionless number for heat transfer studies. It plays a vital role in both forced and natural convection. Nusselt number is also called a dimensionless heat transfer coefficient for convection.

The mathematical expression of local Nusselt number Nu is given below:

$$Nu=-\frac{\partial T}{\partial n}.\qquad(21)$$

Local Nusselt number for the bottom and side heater is given as under:

$$Nu_b=-\frac{\partial T}{\partial y},\quad Nu_l=\frac{1}{\sqrt{2}}\left(-\frac{\partial T}{\partial x}+\frac{\partial T}{\partial y}\right),$$

$$Nu_r=\frac{1}{\sqrt{2}}\left(\frac{\partial T}{\partial x}+\frac{\partial T}{\partial y}\right).\qquad(22)$$

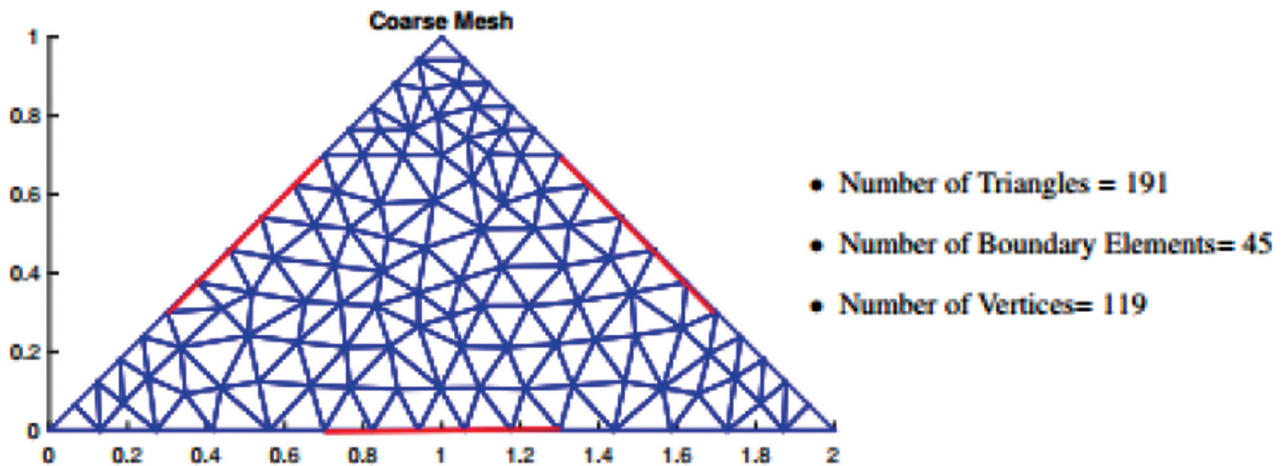**Figure 2.** Coarse mesh and details.

Table 1. Mesh independence test

Number of Triangles	Pr	Re	*Ri*	*β*	N_R	*Nū* (Bottom)	Abs. Error
742	0.7	100	10	0.01	1	−0.03599	–
1651	0.7	100	10	0.01	1	−0.03712	0.0011
2966	0.7	100	10	0.01	1	−0.03732	0.0002
6952	0.7	100	10	0.01	1	−0.03799	0.00067

The relation between average and local Nusselt number can be defined as:

$$\overline{Nu_b} = \frac{5}{3}\int_{0.7}^{1.3} Nu_b \quad dx, \quad \overline{Nu_l} = \frac{2\sqrt{2}}{5}\int_{0.7}^{1.3} Nu_l \quad ds,$$

$$\overline{Nu_r} = \frac{2\sqrt{2}}{5}\int_{0.7}^{1.3} Nu_r \ ds. \tag{23}$$

CODE VALIDATION

To fortify the algorithm, we have tested and validated our code for the previous study of T. Basak, et al. [9], in which uniform and nonuniform heating effect of bottom wall in a lid driven cavity was investigated by keeping the vertical wall at constant temperature. It is noted that our results agree well with the corresponding results reported in [9].

NUMERICAL RESULTS AND DISCUSSION

The nature of the stream function, temperature zone, local and average Nusselt number for certain values of involved parameters are interpreted vividly. From the literature on bi-viscosity flows, the simulation is seized for certain values of parameter Ha, Gr, Re and Ri [16]. The radiation parameter N_R is restricted from $0 \leq N_R \leq 10$ for reference followed by [23]. A similar approach has not been evaluated for the cavities. In the current study, β is taken pretty much in the same manner as taken in reference [16]. The yield stress and shear thinning aspect of
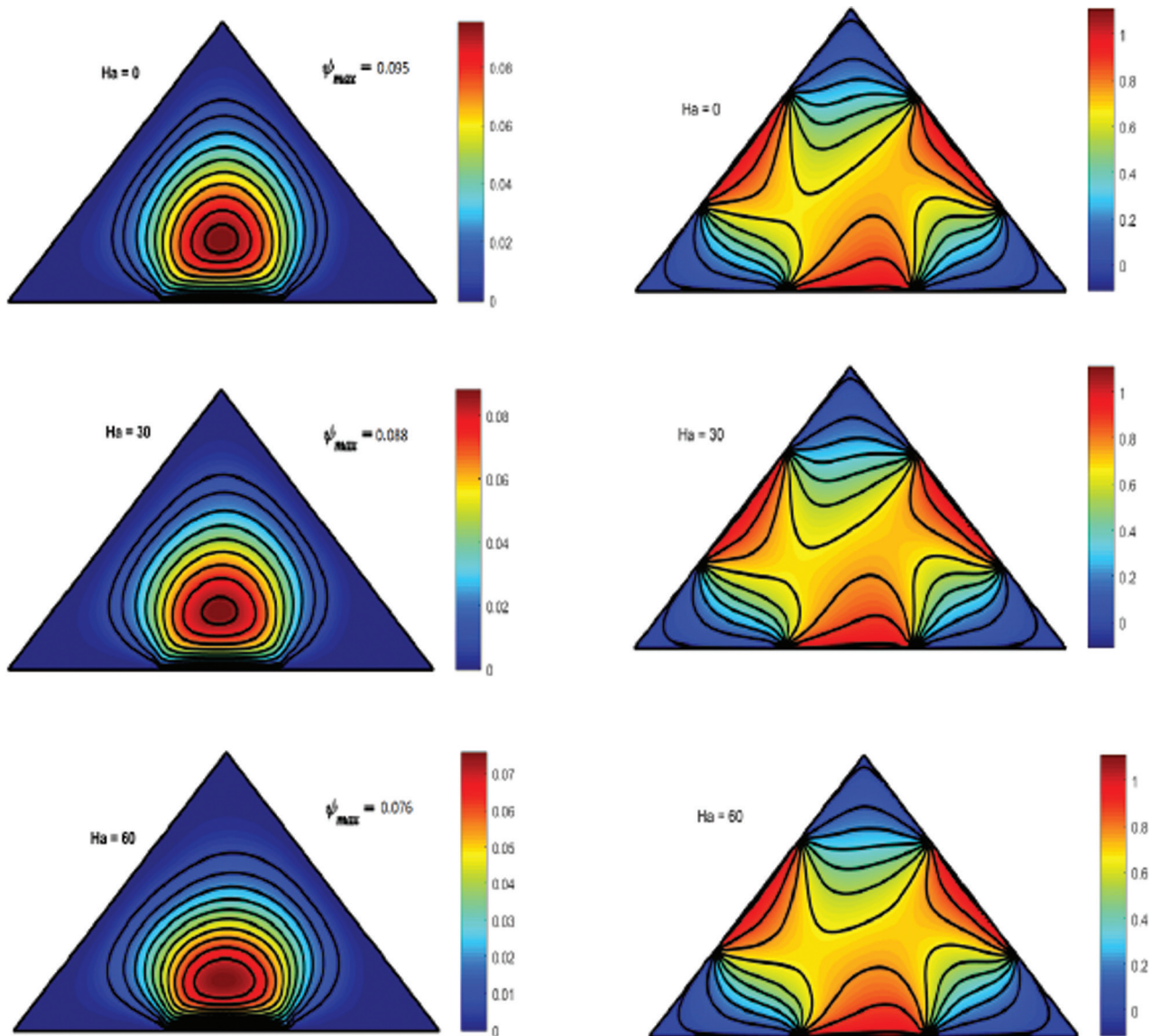

Figure 3. Left: Stream functions Ψ; Right: Isotherms *T*; (*Re* = 10², *Pr* = 0.7, *Ri* = 10, N_R = 1, *Ha* = 0, ∈ = 0.5).

fluid can be elaborated by the bi-viscosity model. Blood slurries are the prevailing examples of bi-viscosity fluid. The Prandtl number Pr for the blood ranges from 10 to above. While there is no presence of Prandtl number ranges for the slurries. That's why the simulations in the current study are carried out for a fluid whose Prandtl ranges from $0 \leq Pr \leq 10$.

Figure 2 is the structure of the coarse mesh of current geometry. It consists of 191 triangles. However, we use the fine mesh consisting of 1651 triangles. Here in Figure 2, the red zone on the wall represents the heater. It clearly shows how we make the distribution of hot and cold walls. The motion of the bottom heater exposed the inertial impact on the bottom wall.

MESH INDEPENDENCE TEST

Figure 3 depicts a direct relationship between bi-viscosity parameter and stream function. For different values of β different patterns of stream, lines are plotted. For $\beta = 0.01$, anticlockwise primary circulation is observed, and maximum value obtained for stream function is 0.094. Secondary circulation is appeared at $\beta = 0.5$ and $\beta = 1$. For $\beta = 0.5$ the value of stream function is 0.14. While in case of $\beta = 1$ the $\psi = 0.17$.

Figure 4 reveals the interesting aspect of current study. For $\beta = 0.01$, the maximum value of stream function which is observed is 0.093. A secondary circulation at $\beta = 0.5$ is detected with same value of stream unction as in the case of $\beta = 0.01$. When the value of bi-viscosity parameter gained
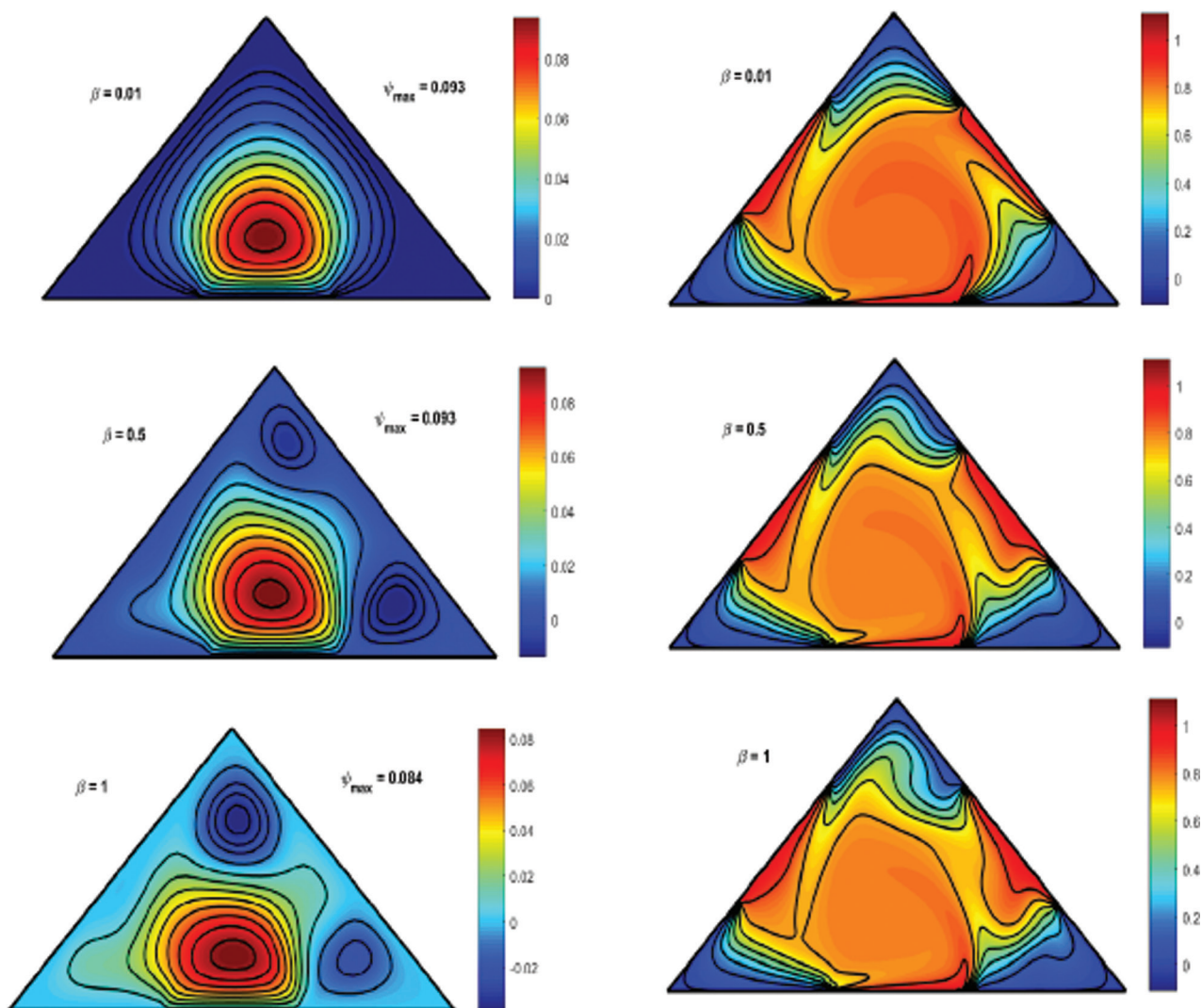

Figure 4. Left: Stream functions Ψ; Right: Isotherms T; ($Re = 10^2$, $Pr = 10$, $Ri = 10$, $N_R = 1$, $Ha = 0$, $\in$ = 0.5).
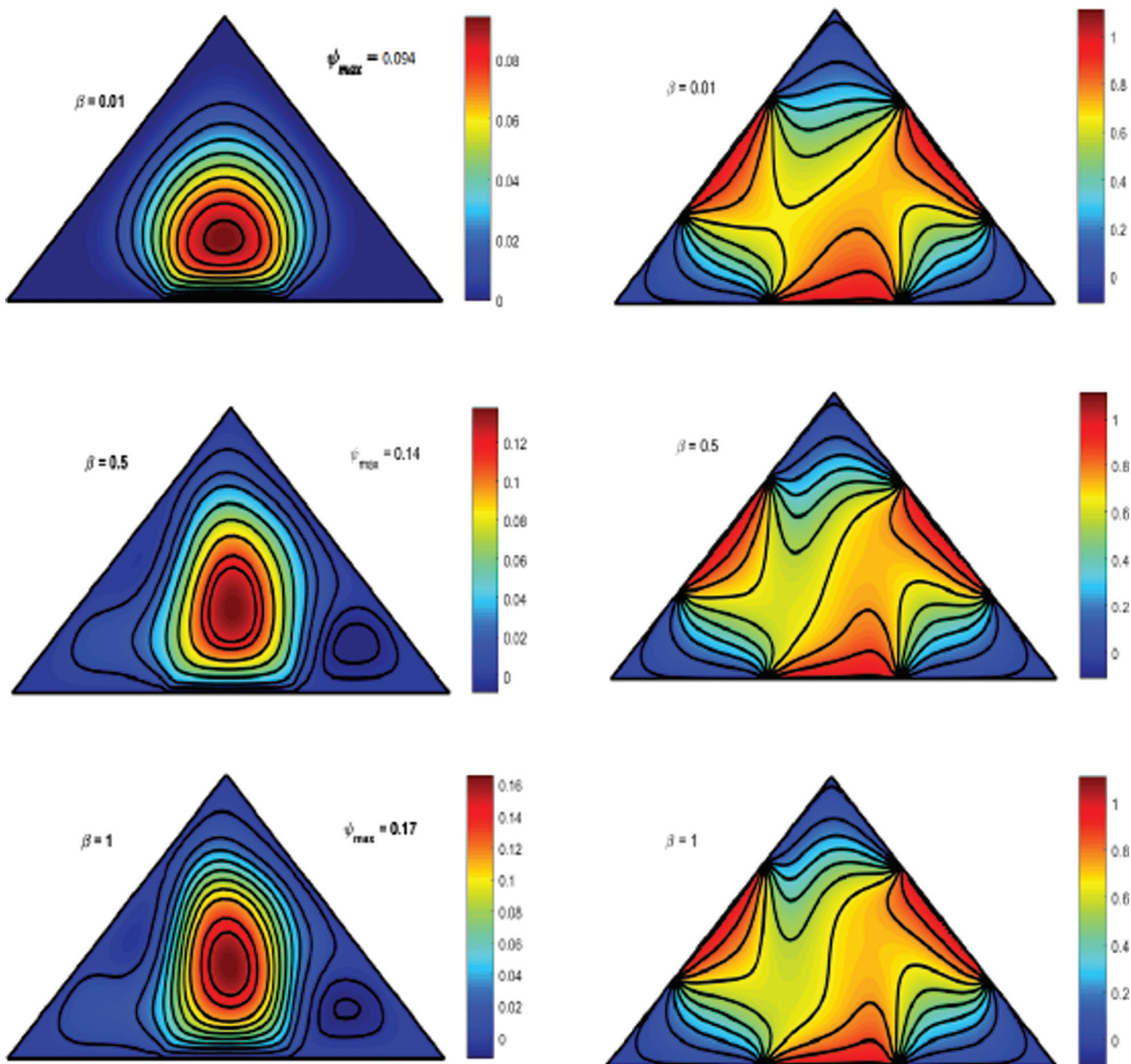
Figure 5. Left: Stream functions Ψ; Right: Isotherms *T*; (*Re* = 10², *Pr* = 0.7, *Ri* = 10, N_R = 1, *β* = 0.03, ∈ = 1).

value 1, a strong anticlockwise secondary circulation is being observed. Stream function showed a low value for *β* = 1 as compared to *β* = 0.5 and *β* = 0.01. These observations are carried out for *Pr* = 10.

From Figure 5 its quite evident that for *Pr* = 0.7 there exists an inverse relationship between Hartmann number and motion of the fluid. For *Ha* = 0 the stream function gives a value of 0.095. An anticlockwise circulation is observed. As we increase the Hartmann number the motion of fluid decreases. For *Ha* = 30 the value of stream function is *ψ* = 0.088, and for *Ha* = 60, *ψ* = 0.076. These observations are made for *Pr* = 0.7.

Figure 6 expounds that for *Pr* = 10, *β* = 0.3, N_R = 1, *Re* = 10² the relationship between Hartmann number and stream function retained as in the previous figure. It can be concluded that an increment in the Hartmann number did not affect the pattern of streamlines in both cases for *Pr* = 0.7 and *Pr* = 10. The anticlockwise behaviour also retained in Figure 6.

Figure 7 displays the stream lines pattern and temperature contour over a wide range of thermal radiation parameter and *Pr* = 0.7 for *Re* = 10² and *β* = 0.05. The anticlockwise secondary circulation is detected for 0 ≤ N_R ≤ 10. For N_R = 5 and N_R = 10 same motion of fluid is observed.

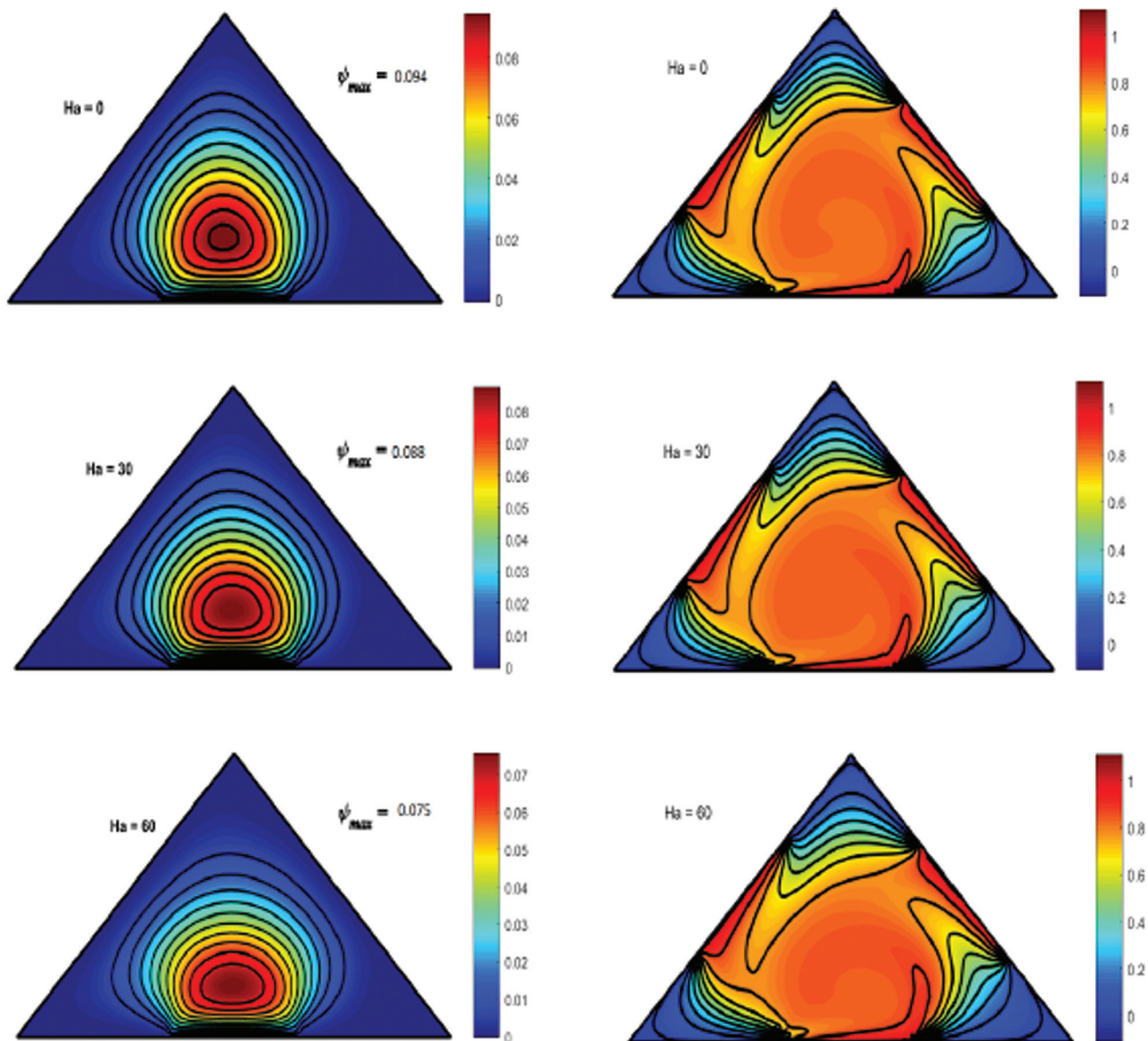**Figure 6.** Left: Stream functions Ψ; Right: Isotherms T; ($Re = 10^2$, $Pr = 10$, $Ri = 10$, $N_R = 1$, $\beta = 0.03$, $\in\, = 1$).

While $N_R = 0$ gives a slightly high value of ψ as compared to other values of thermal radiation parameter.

From Figure 8 it can be noticed that for $Pr = 10$ the relationship between thermal radiation parameter and stream function is inverse. The anticlockwise secondary circulation is recognized. The maximum motion of the fluid is observed for $N_R = 0$. The velocity of motion decreased as the value of the thermal radiation parameter increased.

Figure 9 illustrates the behaviour of the local Nusselt number along the bottom wall of the cavity against the bi-viscosity parameter. For $\beta = 1$ the maximum value of Nusselt number is attained. For $x = 0.7$ all three values

of the bi-viscosity parameter give maximum value of Nusselt number. For $0.75 \leq x \leq 1.05$, the Nusselt number shows the decreasing behaviour. After that graph depicts the increasing behaviour for the interval $1.1 \leq x \leq 1.3$. For $Pr = 10$, it's analysed that for three different values of the bi-viscosity parameter the Nusselt number showed different demeanour than for $Pr = 0.7$ at the bottom wall. The difference between the maximum values of Nusselt number for $\beta = 1$ and $\beta = 0.5$ is comparatively smaller than for $\beta = 0.01$.

At $x = 0.7$ Nusselt number gained its maximum value after that it starts to decrease. For $\beta = 1$ and $\beta = 0.5$ Nusselt number exhibited decreasing behaviour for 0.7
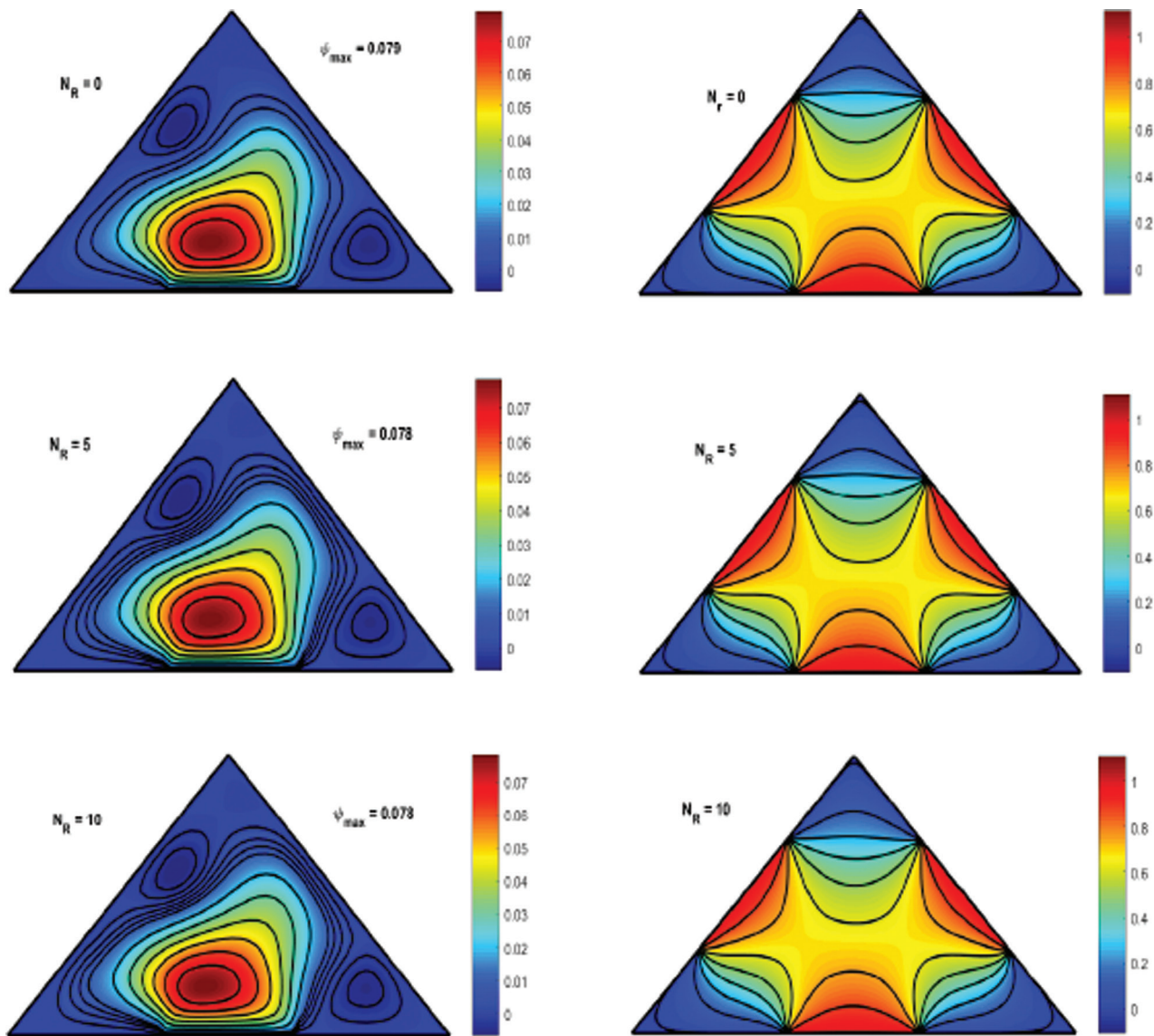
Figure 7. Left: Stream functions Ψ; Right: Isotherms *T*; (*Re* = 10, *Pr* = 0.7, *Ri* = 1000, *Ha* = 60, *β* = 0.05, ∈ = 0.25).

≤ *x* ≤ 1.3. While in the case of *β* = 0.01 Nusselt number decreases in the interval 0.7 ≤ *x* ≤ 1.1 then it starts to increasing for the *x* ranges from 1.1 – 1.3. The effect of the Nusselt number against the bi-viscosity parameter on the left side of the cavity can be vividly recounted. For three different values of *β* behaviour of Nusselt number is recorded. The maximum value of the Nusselt number at y = 0.3 is observed for all three values bi-viscosity parameter. Interval 0.3 ≤ *y* ≤ 0.5 showed a decreasing behaviour of Nusselt number.

While 0.5 ≤ *y* ≤ 0.7 exhibit the increasing behaviour of Nusselt number. These observations are recorded for *Pr* = 0.7. The case for *Pr* = 10 is quite different from the case of *Pr* = 0.7. For *β* = 1 at *y* = 0.3 Nusselt number get its maximum

value then it starts to decrease. A slight increasing behaviour can be observed for 0.6 ≤ *y* ≤ 0.7. The maximum value of Nusselt Number for *β* = 0.01 is higher than for *β* = 0.5 and *β* = 1. The values of Nusselt number for 0.3 ≤ *y* ≤ 0.5 decreases gradually. While for *y* ranges from 0.5 – 0.7 the value of Nusselt number gradually increases. For *β* = 0.5 initially Nusselt number decreases for the interval 0.7 ≤ *y* ≤ 0.45. After that, it shows an increasing behaviour for 0.45 ≤ *y* ≤ 0.7.

Figure 10 elaborate on the nature of the local Nusselt number at *Pr* = 0.7 for the bottom wall of the cavity against the thermal radiation parameter. Graph exhibit the decreasing attitude for the interval 0.7 ≤ *x* ≤ 1. While the interval 1.05 ≤ *x* ≤ 1.3 expounds the increasing behaviour
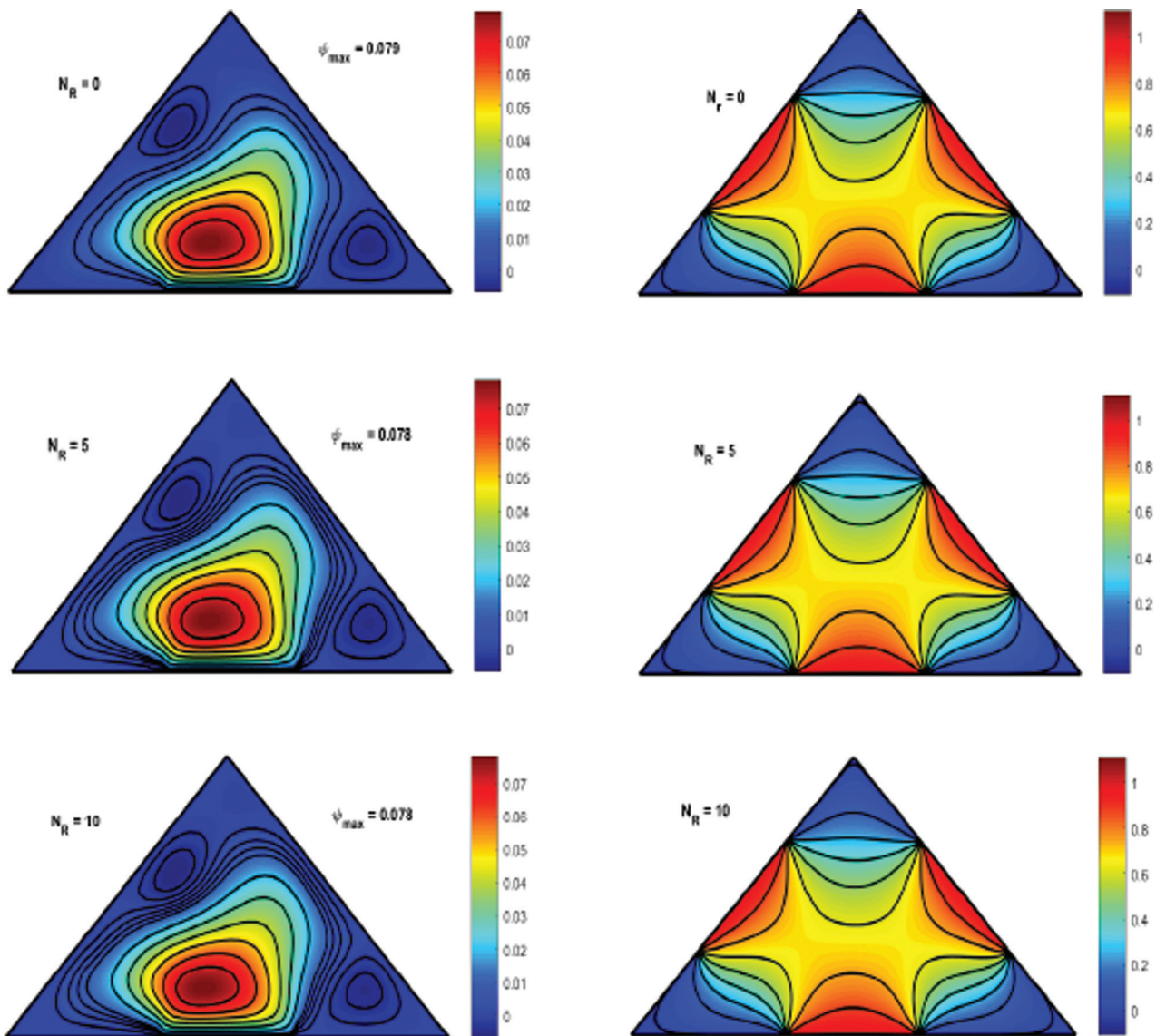
Figure 8. Left: Stream functions Ψ; Right: Isotherms T; ($Re = 10$, $Pr = 10$, $Ri = 1000$, $Ha = 60$, $\beta = 0.05$, $\in = 0.25$).

of Nusselt number. As we increase the Prandtl number from 0.7 to 10, for $N_R = 5$ the Nusselt number attains its maximum value. Initially for $N_R = 0$ the value of Nusselt number at $x = 0.7$ is comparatively higher than for other values of thermal radiation parameter, while for $N_R = 5$ the magnitude of Nusselt number decreases at $x = 0.7$. For interval, $1.08 \leq x \leq 1.3$ the different values of N_R exhibit opposite behaviour of Nusselt number as compared to the initial values. In this interval for $N_R = 5$, Nusselt number gains its maximum value as compared to other values of N_R. While the minimum value is achieved against the $N_R = 0$. Figure 10 also elaborate on the behaviour of local Nusselt number along the sidewall of the cavity for $Pr = 0.7$. At y

= 0.3 Nusselt number attained maximum value against the five different values of N_R. But when y ranges from 0.3 – 0.5 Nusselt number showed decreasing behaviour. While at $y = 0.5$ Nusselt number exhibited its minimum value. For $Pr = 10$ the profile of Nusselt number is quite interesting for $N_R = 5$ initially Nusselt number gained its maximum value as compared to other values of N_R. The behaviour of Nusselt number in the interval $0.3 \leq y \leq 0.45$ is in contrast with interval $0.5 \leq y \leq 0.7$.

The nature of the Nusselt number for the bottom wall of the cavity is plotted against the Hartmann number in the Figure 11. Nusselt number for $Ha = 60$ attained its maximum value and minimum value at $Ha = 0$. The magnitude
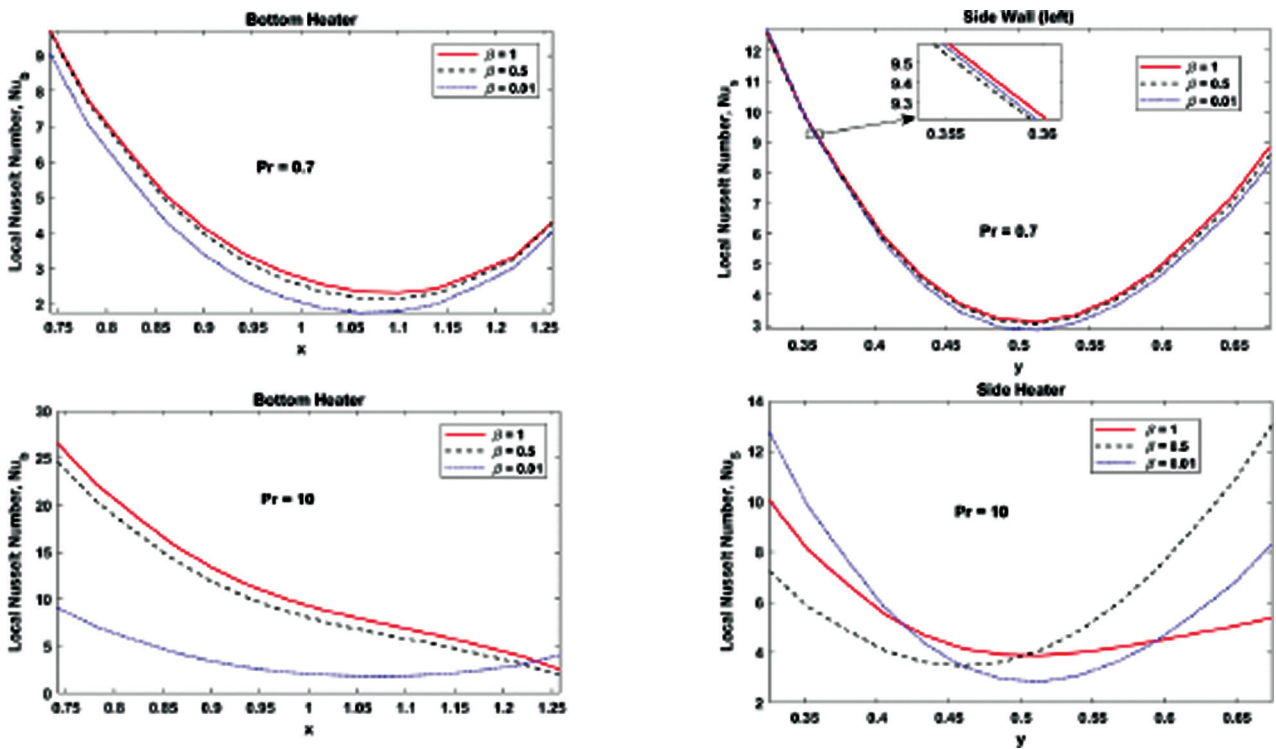
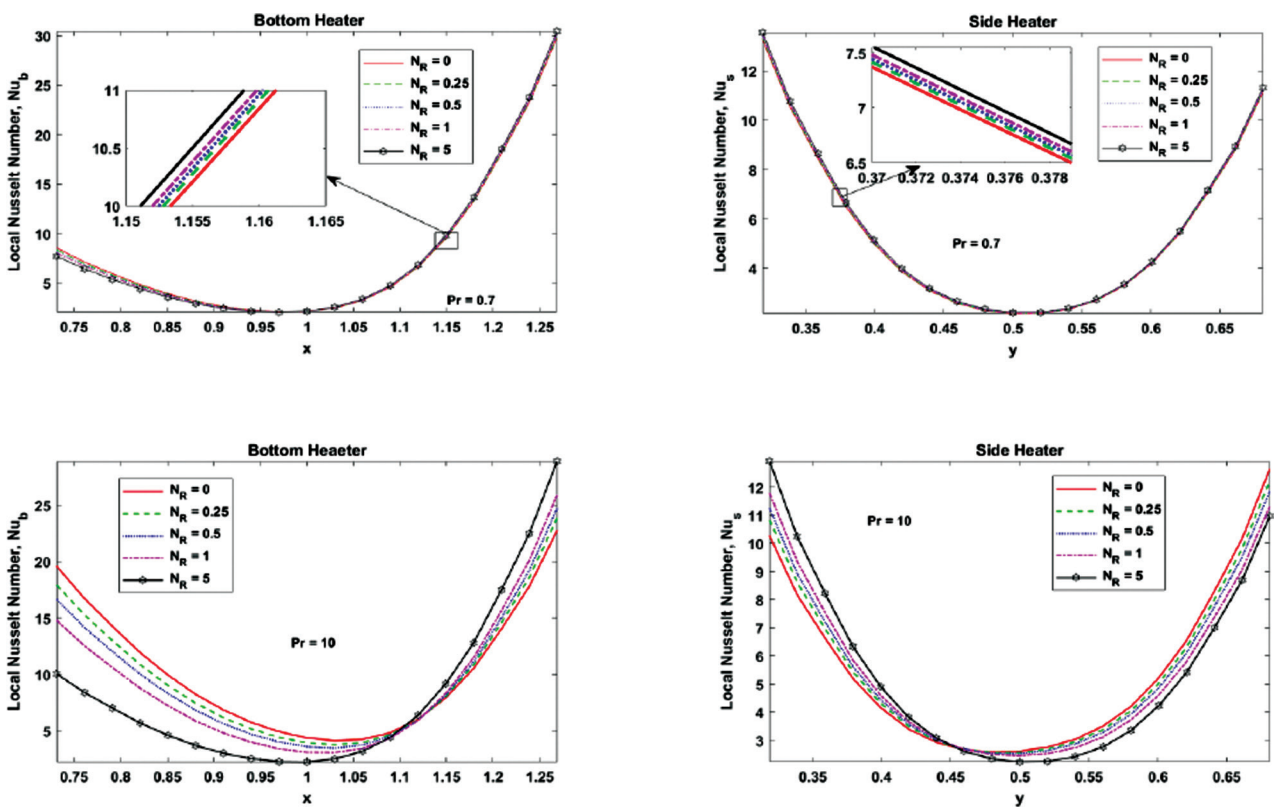**Figure 9.** Local Nusselt number at side and bottom heater, for $Re = 10^2$, $Ri = 10$, $Ha = 0$, $\in = 0.5$.

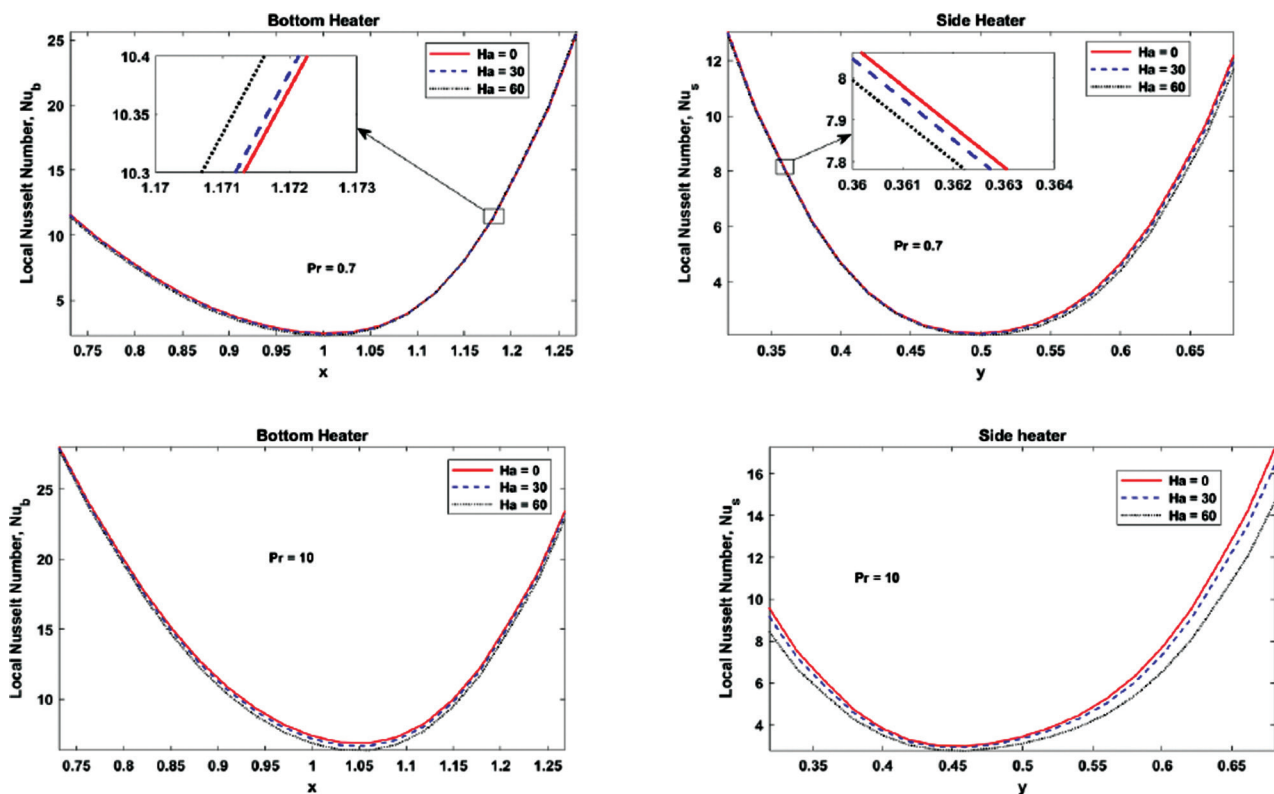**Figure 10.** Local Nusselt number at side and bottom heater, for $Re = 10^2$, $Ri = 10$, $Ha = 0$, $\in = 0.5$.

Figure 11. Local Nusselt number at side and bottom heater, for $Re = 10^2$, $Ri = 10$, $Ha = 0$, $\in = 0.5$.

of Nusselt number in the interval $0.7 \leq x \leq 1$ is analogously smaller than the magnitude in $1 \leq x \leq 1.3$. For $Pr = 10$ the trend of Nusselt number in the interval $0.7 \leq x \leq 1.05$ is decreasing while in the interval $1.05 \leq x \leq 1.3$ its increasing. At $x = 1.05$ minimum value of Nusselt number is achieved for all three values of Hartmann's number. Nusselt number at the sidewall in the interval $0.3 \leq y \leq 0.5$ shows decreasing behaviour while in the interval $0.5 \leq y \leq 0.7$ the profile of Nusselt number exhibit the increasing behaviour. At $y = 0.5$ Nusselt number attained its minimum value against all three values of Hartmann's number. In case of $Pr = 10$ the Nusselt number decreases in the interval $0.3 \leq y \leq 0.45$. While the magnitude of Nusselt number increases in the interval $0.5 \leq y \leq 0.7$.

Figure 12 exhibits the trend of Nusselt number against the heat generation parameter ranges from $-10 \leq \in \leq 10$, for the bottom wall. There exists an inverse relationship between the heat generation parameter and Nusselt number. In the case of $Pr = 0.7$, the value of $\in$ decreases as the magnitude of Nusselt number increases. The maximum value of Nusselt number is achieved in the interval $1 \leq x \leq 1.3$, against the $\in = -10$. While in case of $Pr = 10$, the behaviour of Nusselt number is decreasing in the interval $0.7 \leq y \leq 1$, and increasing in $1 \leq x \leq 1.3$. The profile of

Nusselt number for the side wall of the cavity for $Pr = 0.7$ is decreasing in the interval $0.3 \leq x \leq 0.5$ and increasing in the interval $0.5 \leq y \leq 0.7$. In case of $Pr = 10$ the maximum magnitude of Nusselt number is achieved in the interval $0.45 \leq y \leq 0.7$ and interval $0.3 \leq y \leq 0.45$ return the decreasing act of Nusselt number.

The profile of average Nusselt number against a wide range of Grashof number $10^4 \leq Gr \leq 10^5$ for three different values of the bi-viscosity parameter is analysed for $Pr = 0.7$ in Figure 13. In the case of the bottom wall, the maximum value of the average Nusselt number for $\beta = 1$ is observed against the Grashof number. An approximated constant behaviour of the average Nusselt number is analysed for $\beta = 0.01$. For $\beta = 0.5$ average Nusselt number depicts the almost linear demeanour. The magnitude of the average Nusselt number increased by increasing the $Pr = 0.7$ to 10. The profile of the average Nusselt number for the side wall is also carried out for $Pr = 0.7$ in the Figure 13. In this case, the magnitude of the average Nusselt number linearly increased by increasing the Gr for $\beta = 1$ and 0.5. While the minimum value of the average Nusselt number is achieved for $\beta = 0.01$.

In the case of $Pr = 0.7$, the minimum value of the average Nusselt number is noticed for $\beta = 1$ as it depicts
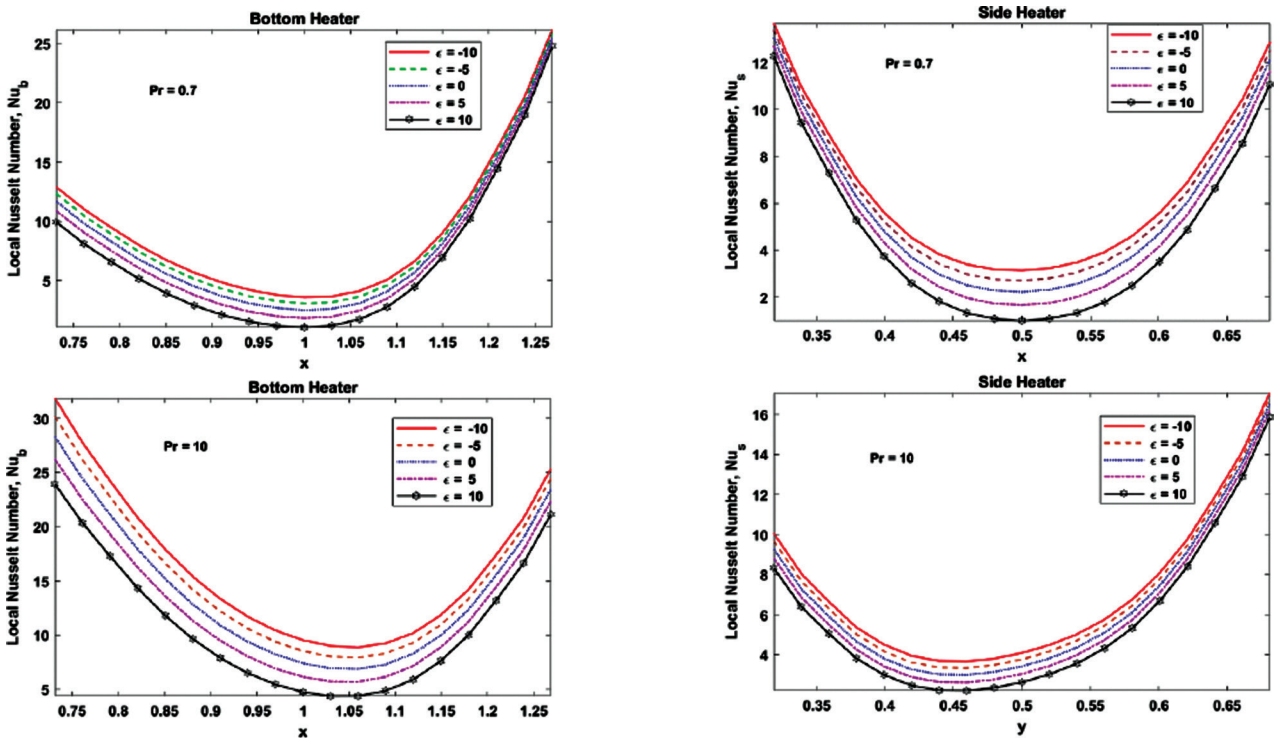
Figure 12. Local Nusselt number at side and bottom heater, for $Re = 10^2$, $Ri = 10$, $Ha = 0$.

Figure 13. Average Nusselt number with Grashof number along the side and bottom heater, for $Re = 10^2$, $Ri = 10$, $Ha = 0$, $\in = 0.5$, $N_R = 1$.

Figure 14. Average Nusselt number with Grashof number along the side and bottom heater, for $Re = 10$, $Ha = 60$, $\in = 0.25$, $\beta = 0.03$.
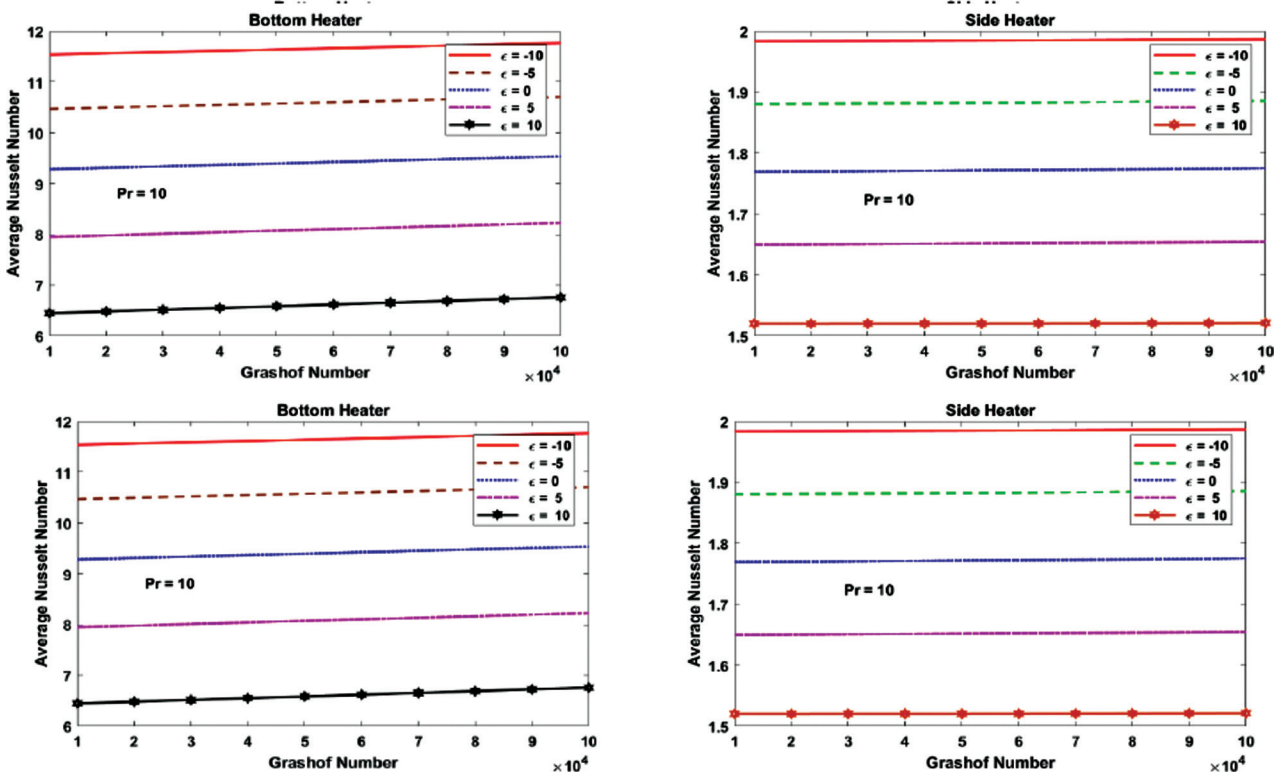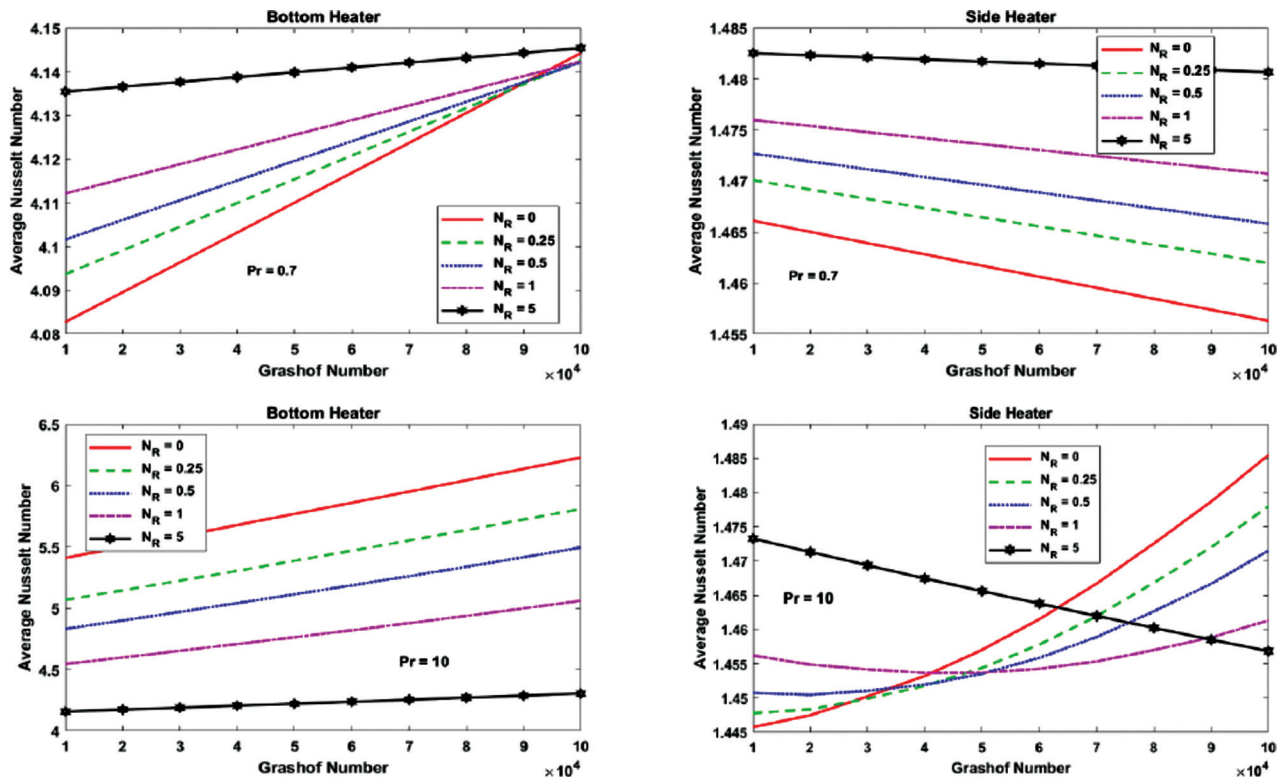
Figure 15. Average Nusselt number with Grashof number along the side and bottom heater, for $Re = 10^2$, $Ri = 10$, $Ha = 30$, $N_R = 1$.

the linearly decreasing demeanour. For side wall heater, the maximum value of the average Nusselt number is observed for β = 0.5. While β = 0.01 retained its behaviour and gives almost a constant value of average Nusselt number.

Figure 14 illustrate the trend of average Nusselt number against the broad range of thermal radiation parameter. For Pr = 0.7 observations are carried out for the bottom and sidewall of the cavity. In the case of the bottom wall for Pr = 0.7 and 10, the average Nusselt number showed a linearly increasing trend. While in the case of side wall heater for Pr = 0.7 average Nusselt number depicts the decreasing behaviour. As we increase the value of Prandtl number Pr = 10 a little bit different demeanour of Nusselt number is recognized.

The values of Nusselt number linearly increase for thermal radiation parameter ranges from $0 \leq N_R \leq 1$. But in the case of N_R = 5 the average Nusselt number illustrates a decreasing behaviour.

Figure 15 demonstrate the profile of the average Nusselt number over a wide range of heat generation parameter. In both cases of the bottom and side wall for Pr = 0.7 and Pr = 10, an increasing trend is noticed.

CONCLUSION

The analysis is carried out for the study of a bi-viscosity fluid through mixed convection in a triangular cavity under the influence of heating and magnetic effects. The uniformly discrete heating effect is applied at the center of each wall. The heater at the bottom wall is assumed to be moving along positive x-direction. While the heaters at the inclined walls are kept fixed. The numerical simulations of governing equations are carried out by using the standard Galerkin Finite Element Method. Based on the obtained results in the present study, the important conclusions are drawn as follow:

- By increasing the magnitude of a bi-viscosity parameter, secondary circulation is observed for convection dominate case. The rate of heat transfer has a direct relation with the bi-viscosity parameter.
- For thermal radiation parameter N_R, strong secondary circulations are spotted for Pr = 0.7,10.
- For the different value of Hartmann's number, only primary circulations are observed in both cases (Pr = 0.7,10).
- The maximum value of local and average Nusselt number is observed for convection dominate case at the bottom wall of the cavity against the heat generation parameter $\in$ = –10.
- Maximum value of stream function is observed for Pr = 0.7 at β = 1, while the minimum value is noticed against the Hartmann number Ha = 60 for convection dominate case.

- For convection dominate case a slight difference can be seen in the isotherms for Hartmann number, thermal radiation, and bi-viscosity parameter, while in the case of Pr = 0.7 the effect of Hartmann number, bi-viscosity and thermal radiation parameter on the isotherm is negligible.

The results conferred that the settings of the properties of the fluid are the key role to achieve the desired thermal effects. Maximum intensity of circulation was observed for large value of bi-viscosity parameter i.e. β = 1, for Pr = 0.7. A significant change in isotherm is observed for Pr = 10, by increasing the value of the bi-viscosity parameter β, and Hartmann's number Ha. Hence, the bi-viscosity parameter should be large to improve the thermal operations of fluid.

NOMENCLATURE

$\vec{A}$	Rate of strain tensor
Nu	Local Nusselt number
$N\bar{u}$	Average Nusselt number
k^*	Mean absorption coefficient
c_p	Specific heat of the fluid.
N_R	Radiation parameter
P_y	Yield stress parameter

Greek symbols

α	Thermal diffusivity, m²·s⁻¹
β	Bi-viscosity parameter
ϕ	Solid volume friction
σ	Stefan Boltzmann constant
μ	Dynamic viscosity, kg.m⁻¹·s⁻¹
ρ	Density of the fluid
$\in$	Heat generation parameter
ψ	Dimensionless stream function
γ	Penalty parameter
π	Second invariant of strain tensor
π_c	Critical value of π
θ_h	Hot wall temperature
θ_c	Cold wall temperature
η_1, η_2, η_3	Trail functions

Dimensionless parameter

T	Temperature
P	Pressure
Re	Reynold number
Pe	Peclet number
Ri	Richardson number
Ha	Hartmann number
Gr	Grashof number
Pr	Prandtl number
Da	Darcy number

Subscripts

R	Refers to radiations

y	Refers to yield
c	Refers to critical values
h	Refers to hot

AUTHORSHIP CONTRIBUTIONS

Authors equally contributed to this work.

DATA AVAILABILITY STATEMENT

The authors confirm that the data that supports the findings of this study are available within the article. Raw data that support the finding of this study are available from the corresponding author, upon reasonable request.

CONFLICT OF INTEREST

The author declared no potential conflicts of interest with respect to the research, authorship, and/or publication of this article.

ETHICS

There are no ethical issues with the publication of this manuscript.

REFERENCES

[1] Bondareva NS, Sheremet MA. Numerical simulation of natural convection melting in 2d and 3d enclosures. J Therm Eng 2019:5;51–61. [CrossRef]

[2] Sivakumar V, Sivasankaran S, Prakash P, Lee J. Effect of heating location and size on mixed convection in lid-driven cavities. Comput Math with Appl 2010:59;3053–3065. [CrossRef]

[3] Mohamad AA, Viskanta R. Flow and heat transfer in a lid-driven cavity filled with a stably stratified fluid. Appl Math Model 1995:19;465–472. [CrossRef]

[4] Mahapatra TR, Pal D, Mondal S. Mixed convection flow in an inclined enclosure under magnetic field with thermal radiation and heat generation. Int Commun Heat Mass Transf 2013:41;47–56. [CrossRef]

[5] Basak T, Roy S, Sharma PK, Pop I. Analysis of mixed convection flows within a square cavity with linearly heated side wall(s). Int J Heat Mass Transf 2009:52;2224–2242. [CrossRef]

[6] Basak T, Roy S, Singh SK, Pop I. Analysis of mixed convection in a lid-driven porous square cavity with linearly heated side wall(s). Int J Heat Mass Transf 2010:53;1819–1840. [CrossRef]

[7] Bhattacharya M, Basak T, Oztop HF,Varol Y. Mixed convection and role of multiple solutions in lid-driven trapezoidal enclosures. Int J Heat Mass Transf 2013:63;366–388. [CrossRef]

[8] Ching YC, Oztop HF, Rahman MM, Islam MR, Ahsan A. Finite element simulation of mixed convection heat and mass transfer in a right triangular enclosure. Int Commun Heat mass Transf 2012:39;689–696. [CrossRef]

[9] Basak T, Roy S, Sharma PK, Pop I. Analysis of mixed convection flows within a square cavity with uniform and non-uniform heating of bottom wall. Int J Therm. Sci 2009:48;891–912. [CrossRef]

[10] Hasanuzzaman. M, Rahman MM, Oztop HF, Rahim NA,Saidur R. Effects of Lewis number on heat and mass transfer in a triangular cavity. Int Commun Heat Mass Transf 2012:39;1213–1219. [CrossRef]

[11] Turkyilmazoglu M. Analytical solutions to mixed convection mhd fluid flow induced by a nonlinearly deforming permeable surface. Commun Nonlinear Sci Numer Simul 2018:63;373–379. [CrossRef]

[12] Sivasankaran S, Sivakumar V, Hussein AK. Numerical study on mixed convection in an inclined lid-driven cavity with discrete heating. Int Commun Heat Mass Transf 2013:46;112–125. [CrossRef]

[13] Selimefendigil F, Oztop HF. MHD mixed convection and entropy generation of power law fluids in a cavity with a partial heater under the effect of a rotating cylinder. Int J Heat Mass Transf 2016:9840–9851. [CrossRef]

[14] Sebdani SM, Mahmoodi MM, Hashemi SM. Effect of nanofluid variable properties on mixed convection in a square cavity. Int J Therm Sci 2012:52;112–126. [CrossRef]

[15] Rahman MM, Oztop HF, Saidur R, Mekhilef S, Al-Salem K. Finite element solution of MHD mixed convection in a channel with a fully or partially heated cavity. Comput Fluids 2013:79;53–64. [CrossRef]

[16] Ali N, Nazeer M, Javed T, Razzaq M. Finite element analysis of bi-viscosity fluid enclosed in a triangular cavity under thermal and magnetic effects. Eur Phys J Plus 2019:134;12448. [CrossRef]

[17] Das D, Lukose L, Basak T, Role of multiple discrete heaters on the entropy generation during natural convection in porous square and triangular enclosures. Numer Heat Transf A Appl 2018:74;1636–1665. [CrossRef]

[18] Das D, Lukose L, Basak T. Analysis of efficiency of convection in porous geometries (square vs triangular) with multiple discrete heaters on walls: A heatline perspective. Int J Numer Methods Heat Fluid Flow 2019:29;3305–3346. [CrossRef]

[19] Das D, Basak T. Role of distributed/discrete solar heaters during natural convection in the square and

triangular cavities: CFD and heatline simulations. Sol Energy 2016:35;130–153. [CrossRef]

[20] Arthur EM, Seini IY, Bortteir LB. Analysis of Casson Fluid Flow over a Vertical Porous Surface with Chemical Reaction in the Presence of Magnetic Field. J Appl Math Phys 2015:3;713–723. [CrossRef]

[21] Turek S, Hron J, Razzaq M. Numerical benchmarking of fluid-structure interaction between elastic object and laminar incompressible flow. Dortmund Univ, 2010.

[22] Weichert F, Walczak L, Fisseler D, Opfermann T, Razzaq M, Münster R et al; Simulation of Intra-Aneurysmal Blood Flow by Different Numerical Methods. Comput Math Methods Med 2013:2013;527654. [CrossRef]

[23] M. S. Astanina, M. A. Sheremet, and J. C. Umavathi, Effect of thermal radiation on natural convection in a square porous cavity filled with a fluid of temperature-dependent viscosity. Therm Sci 2018:22;391–399. [CrossRef]